Available online at www.sciencedirect.com
SCIENCE DIRECT®
Acta Materialia 52 (2004) 3707–3719
Acta MATERIALIA
www.actamat-journals.com

Ratcheting-induced wrinkling of an elastic film on a metal layer under cyclic temperatures

S.H. Im, R. Huang *

Department of Aerospace Engineering and Engineering Mechanics, Research Center for Mechanics of Solids, Structures and Materials, The University of Texas, Austin, TX 78712, USA

Received 3 March 2004; received in revised form 5 April 2004; accepted 26 April 2004
Available online 25 May 2004

Abstract

This paper develops a theoretical model for wrinkling of an elastic film on an elastic–plastic metal layer caused by cyclic temperatures. The film is compressively strained and bonded to the metal layer, which in turn lies on a thick substrate. The thermal expansion mismatch between the metal and the substrate induces a biaxial stress, which is assumed to be large enough to cause the metal to deform plastically during each cycle. Wrinkling of the film induces normal and shear tractions at the film–metal interface, which bias the plastic flow of the metal. Consequently, the metal ratchets, namely, accumulates plastic deformation in the same directions as the temperature cycles. Concomitantly, the wrinkle of the film grows. The model reveals an analogy between ratcheting and creep. Analytical solutions are obtained for linear perturbation analysis and equilibrium states. Numerical simulations show evolution of wrinkles under various conditions and the effect of elastic constraint.

Keywords: Layered structures; Buckling; Ratcheting

1. Introduction

Under in-plane compression, a freestanding membrane tends to buckle. For a thin film bonded to a substrate, the buckling is constrained. If the substrate is elastic and relatively compliant, the film may still buckle into an equilibrium state [1–4], which is often called wrinkling as the wavelength is usually shorter than buckling of a free standing film. If the substrate creeps, the wrinkling becomes a kinetic process, where the amplitude grows over time [5–11]. At high temperatures, interfacial diffusion may also facilitate wrinkling [12]. This paper studies another mechanism of wrinkling, which is induced by ratcheting plastic deformation under cyclic temperatures. Wrinkling of thin films may cause failure in layered structures or produce ordered patterns for micro and nano fabrication.

Thermal cycling is widely used in the microelectronics industry as a test to qualify new products. Various failure modes have been observed after cycling a device between two temperatures for hundreds and thousands of times. Understanding these failure modes is urgently needed in order to interpret the qualification test and to guide new designs. In particular, metal film crawling has been observed for over two decades [13–15]. Metal films, serving as interconnects in microelectronic devices, crawl toward the die center as the temperature cycles, resulting in excessive deformation near the die corners, sometimes even cracking adjacent passivation layers. The mechanism of metal film crawling as well as the induced cracking has been recently explained using the concept of ratcheting [16–19]. The deformation in the same direction caused by a cyclic load (e.g., temperature cycle) is known as ratcheting [20–22], which has been observed in many engineering structures. The ratcheting deformation in the metal films builds up stresses in the brittle passivation layers and leads to cracking. An analogy between ratcheting and creep has been

* Corresponding author. Tel.: +1-512-471-7558; fax: +1-512-471-5500.
E-mail address: ruihuang@mail.utexas.edu (R. Huang).

1359-6454/$30.00 © 2004 Published by Elsevier Ltd on behalf of Acta Materialia Inc.
doi:10.1016/j.actamat.2004.04.025

developed to understand the kinetics of ratcheting-induced crack initiation and growth [18,23,24].

The analogy between ratcheting and creep suggests that, under certain conditions, a compressively strained elastic film on a metal layer may wrinkle due to the plastic ratcheting deformation of the metal under cyclic temperatures, as it would on a creeping substrate [5–11]. Indeed, studies of thermal barrier systems have shown that, upon thermal cycling, the thin film of thermally grown oxide (TGO) wrinkles [10,25–28]. Fig. 1 shows a schematic of a typical thermal barrier system, consisting of a thick superalloy substrate, a metal alloy bond coat, a TGO film, and a ceramic thermal barrier coat (TBC). Wrinkling of the TGO film may lead to various failure modes, such as delamination at the interfaces and cracking of the ceramic TBC. The mechanism of wrinkling, however, has not been fully understood due to a large number of factors that potentially play roles in the wrinkling process. He et al. [25] carried out a numerical analysis, showing that ratcheting occurs when the initial wrinkle amplitude exceeds a critical value. In their analysis, they neglected the thermal expansion mismatch between the bond coat and the superalloy substrate. Karlsson and Evans [27] relaxed this limitation and showed enhanced ratcheting. Recent experiments have indicated that thermal expansion mismatch between the bond coat and the superalloy plays an important role in the wrinkling process [29].

In this paper, we present a theoretical model that predicts ratcheting-induced wrinkling without requiring any critical amplitude. The paper is organized as follows. Section 2 develops the model for an ideal structure (Fig. 2). Differing from the previous studies, the model assumes a large thermal expansion mismatch between the metal layer and the substrate. We demonstrate an analogy between ratcheting and creep, similar to that for metal film crawling [18]. Section 3 presents analytical solutions for linear perturbation analysis and constrained equilibrium states. In Section 4, numerical simulations are conducted to show the evolution of wrinkles under various conditions. Section 5 concludes with remarks on the implications and the limitations of the model.

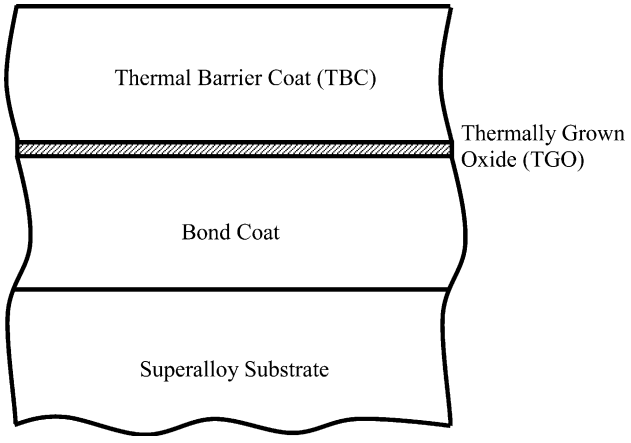

Fig. 1. Schematic of a typical thermal barrier system.

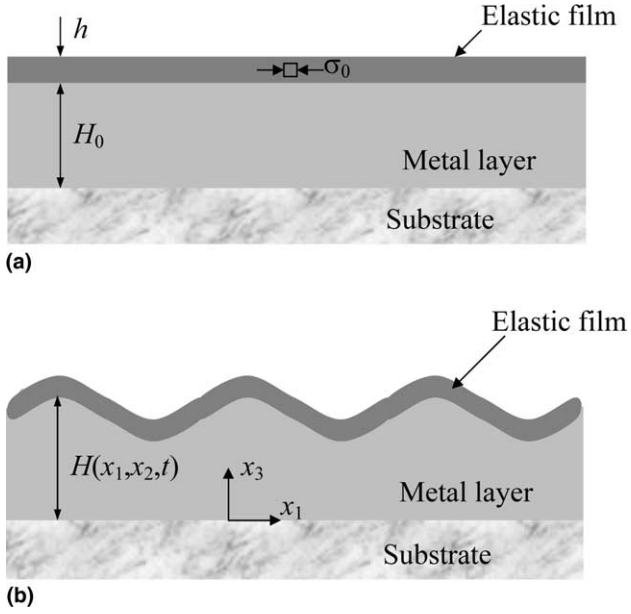

Fig. 2. Schematic of an ideal structure with a compressed elastic film on a metal layer: (a) reference state; (b) wrinkled state.

2. Model formulation

Fig. 2 shows the schematic of an ideal structure: an elastic film of thickness h lies on a metal layer of average thickness H_0, which in turn lies on a thick substrate. At the reference state (Fig. 2(a)), both the elastic film and the metal layer are flat, and the film is subjected to an in-plane biaxial stress σ_0. At the wrinkled state (Fig. 2(b)), the film undergoes in-plane and out-of-plane displacements, and the metal layer deforms accordingly. The thick substrate is assumed to be rigid. The interface between the elastic film and the metal layer is assumed to be perfectly bonded with no separation or sliding. That is, the displacements and the tractions are continuous across the interface. Let w be the deflection (out-of-plane displacement) of the film, u_α the in-plane displacement ($\alpha = 1, 2$), p the pressure (negative normal traction) at the interface, and τ_α the shear tractions. Employing the non-linear von Karman plate theory [30,31] to account for large deflection of the film, equilibrium requires that:

$$p = D_f \frac{\partial^4 w}{\partial x_\alpha \partial x_\alpha \partial x_\beta \partial x_\beta} - N_{\alpha\beta} \frac{\partial^2 w}{\partial x_\alpha \partial x_\beta} - \tau_\alpha \frac{\partial w}{\partial x_\alpha}, \tag{1}$$

$$\tau_\alpha = \frac{\partial N_{\alpha\beta}}{\partial x_\beta}, \tag{2}$$

where

$$D_{\mathrm{f}} = \frac{E_{\mathrm{f}} h^3}{12(1-\nu_{\mathrm{f}}^2)}, \tag{3}$$

$$N_{\alpha\beta} = \sigma_0 h \delta_{\alpha\beta} + E_{\mathrm{f}} h \left[\frac{1}{1+\nu_{\mathrm{f}}} \varepsilon_{\alpha\beta} + \frac{\nu_{\mathrm{f}}}{1-\nu_{\mathrm{f}}^2} \varepsilon_{\gamma\gamma} \delta_{\alpha\beta} \right], \tag{4}$$

$$\varepsilon_{\alpha\beta} = \frac{1}{2}\left(\frac{\partial u_\alpha}{\partial x_\beta} + \frac{\partial u_\beta}{\partial x_\alpha} \right) + \frac{1}{2} \frac{\partial w}{\partial x_\alpha} \frac{\partial w}{\partial x_\beta}. \tag{5}$$

In the above equations, E_{f} is the Young's modulus of the film, ν_{f} the Poisson's ratio, D_{f} the flexural rigidity, $N_{\alpha\beta}$ the in-plane membrane force, $\varepsilon_{\alpha\beta}$ the in-plane strain, $\delta_{\alpha\beta}$ the Kronecker delta. The Greek subscripts α and β take on the values of in-plane coordinates 1 and 2, and a repeated Greek subscript implies summation over 1 and 2. We assume that the film remains elastic during thermal cycles with temperature-independent Young's modulus and Poisson's ratio. The residual stress in the film is also assumed to be temperature-independent, which is a reasonable approximation if the thermal expansion mismatch between the film and the substrate is small (i.e., $\alpha_{\mathrm{f}} \approx \alpha_{\mathrm{s}}$).

The stress state in the metal layer consists of two parts: one is due to thermal expansion mismatch between the metal and the substrate, and the other is due to the tractions at the film–metal interface. At the reference state (Fig. 2(a)), the interface tractions are zero and the metal layer is under a biaxial thermal stress only. With a small perturbation of the interface in the form of wrinkling, the tractions, given by Eqs. (1) and (2), superimpose the thermal stress in the metal. Assume that the interface tractions are small compared to the yield stress of the metal, but the thermal stress by itself is large enough to cause the metal to yield plastically. Let α_{m} and α_{s} be the thermal expansion coefficients of the metal layer and the substrate, respectively. The deformation compatibility between the metal layer and the substrate requires that

$$\mathrm{d}\varepsilon^{\mathrm{p}} + \mathrm{d}\varepsilon^{\mathrm{e}} + \alpha_{\mathrm{m}}\,\mathrm{d}T = \alpha_{\mathrm{s}}\,\mathrm{d}T, \tag{6}$$

where ε^{p} and ε^{e} are the plastic and elastic in-plane strain in the metal layer, respectively, and T is the temperature. We assume that the metal does not creep within the temperature range. Hooke's law relates the incremental elastic in-plane strain to the incremental thermal stress, namely

$$\mathrm{d}\varepsilon^{\mathrm{e}} = \frac{1-\nu_{\mathrm{m}}}{E_{\mathrm{m}}}\,\mathrm{d}\sigma_{\mathrm{T}}, \tag{7}$$

where E_{m} is the Young's modulus of the metal and ν_{m} is the Poisson's ratio.

When the metal is elastic $\mathrm{d}\varepsilon^{\mathrm{p}} = 0$, and a combination of Eqs. (6) and (7) gives the thermal stress increment

$$\mathrm{d}\sigma_{\mathrm{T}} = -\frac{E_{\mathrm{m}}}{1-\nu_{\mathrm{m}}}(\alpha_{\mathrm{m}} - \alpha_{\mathrm{s}})\,\mathrm{d}T. \tag{8}$$

We adopt the J_2 flow theory [32] to analyze the plastic deformation in the metal layer. Assume that the metal is elastic and perfectly plastic with a uniaxial yield strength, Y, independent of the temperature. For a flat metal layer with no tractions at the surface, the Mises yield condition dictates that the metal yields when $\sigma_{\mathrm{T}} = \pm Y$. The thermal stress by itself causes cyclic plastic deformation, but not ratcheting, i.e., the net deformation after one cycle is zero. The tractions at the film–metal interface perturb the stress state in the metal layer. To the first-order approximation, we assume that the pressure at the interface introduces a normal stress in the thickness direction, i.e., $\sigma_{33} = -p$, and neglect the relatively small shear tractions for now. Under these assumptions, the in-plane stresses in the metal layer at yield become

$$\sigma_{11} = \sigma_{22} = \sigma_{\mathrm{T}} = -p \pm Y. \tag{9}$$

In addition, the equilibrium of the metal layer requires that

$$\frac{\partial \sigma_{3\alpha}}{\partial x_3} = \frac{\partial p}{\partial x_\alpha}, \tag{10}$$

where $\sigma_{3\alpha}$ is the shear stress necessary to balance the variation of the in-plane normal stresses in (9). Integrating (10) with respect to x_3 and setting $\sigma_{3\alpha} = \tau_\alpha$ at the film–metal interface ($x_3 = H$), we obtain that

$$\sigma_{3\alpha} = \tau_\alpha - \frac{\partial p}{\partial x_\alpha}(H - x_3), \tag{11}$$

where H is the thickness of the metal layer at the wrinkled state, i.e., $H = H_0 + w$. Note that the shear stresses in (11) vary linearly across the thickness of the metal layer. The shear stresses are small and their contribution to the yielding condition has been neglected. It is cautioned that the above approximation is limited to situations where the metal thickness is small compared to the wavelength of the wrinkle.

The J_2 flow theory dictates that the plastic strain increment be in the same direction as the deviatoric stress tensor, namely, $\mathrm{d}\varepsilon^{\mathrm{p}}_{ij} = (\sigma_{ij} - \frac{1}{3}\sigma_{kk}\delta_{ij})\,\mathrm{d}\lambda$, where $\mathrm{d}\lambda$ is a scalar factor of proportionality. Consequently, we have

$$\frac{\mathrm{d}\varepsilon^{\mathrm{p}}}{\frac{1}{3}(\sigma_{\mathrm{T}} + p)} = \frac{\mathrm{d}\varepsilon^{\mathrm{p}}_3}{-\frac{2}{3}(\sigma_{\mathrm{T}} + p)} = \frac{\mathrm{d}\gamma^{\mathrm{p}}_\alpha}{2\sigma_{3\alpha}}, \tag{12}$$

where $\varepsilon^{\mathrm{p}}_3$ is the plastic strain in the thickness direction, and $\gamma^{\mathrm{p}}_\alpha = 2\varepsilon^{\mathrm{p}}_{3\alpha}$ is the plastic shear strain. No summation over α is noted in (12).

When the metal yields, without hardening, $\mathrm{d}\varepsilon^{\mathrm{e}} = 0$, and from (6)

$$\mathrm{d}\varepsilon^{\mathrm{p}} = -(\alpha_{\mathrm{m}} - \alpha_{\mathrm{s}})\,\mathrm{d}T. \tag{13}$$

Inserting (13) into (12), we obtain that:

$$\mathrm{d}\varepsilon^{\mathrm{p}}_3 = 2(\alpha_{\mathrm{m}} - \alpha_{\mathrm{s}})\,\mathrm{d}T, \tag{14}$$

$$\mathrm{d}\gamma^{\mathrm{p}}_\alpha = -6(\alpha_{\mathrm{m}} - \alpha_{\mathrm{s}})\frac{\sigma_{3\alpha}}{\sigma_{\mathrm{T}} + p}\,\mathrm{d}T. \tag{15}$$

Eqs. (13)–(15) are important for understanding the ratcheting behavior. Assume $\alpha_m > \alpha_s$ for no ambiguity. Start from a low temperature T_L. As the temperature increases ($dT > 0$), the metal first deforms elastically and then yields in compression ($\sigma_T + p = -Y$). Further increasing the temperature causes the metal to flow plastically: the plastic in-plane strain decreases ($d\varepsilon^p < 0$), the plastic thickness strain increases ($d\varepsilon_3^p > 0$), and the plastic shear strain flows in the direction of the shear stress $\sigma_{3\alpha}$. Next, decrease the temperature ($dT < 0$) after reaching a high temperature T_H ($T_H > T_L$). Again, the metal first deforms elastically (unloading) and then yields in tension ($\sigma_T + p = Y$). Upon yielding, the plastic in-plane strain increases ($d\varepsilon^p > 0$), the plastic thickness strain decreases ($d\varepsilon_3^p < 0$), and the plastic shear strain flows again in the direction of the shear stress $\sigma_{3\alpha}$. Consequently, after one cycle, the net increments of both the plastic in-plane strain and the plastic thickness strain are zero. However, since the direction of the shear stress $\sigma_{3\alpha}$ does not change, the plastic shear strain flows in the same direction at both heating and cooling. After each cycle, the plastic shear strain increases by a finite amount, and the metal ratchets. Same ratcheting behavior occurs for $\alpha_s > \alpha_m$.

Fig. 3(a) shows a prescribed temperature cycle, and Fig. 3(b) shows the corresponding in-plane stress. The initial stress at A only affects the first cycle. Integrating

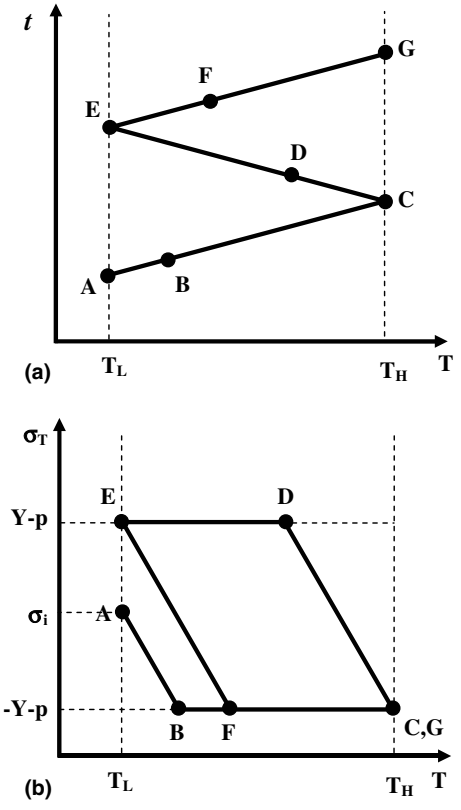

Fig. 3. (a) Prescribed temperature changes with time. (b) In-plane stress as a function of temperature.

(15) over one cycle (e.g., CDEFC) and neglecting the changes of the shear stresses $\sigma_{3\alpha}$ and the pressure p within one cycle, we obtain the net increment of the plastic shear strain per cycle

$$\frac{\partial \gamma_\alpha^p}{\partial N} = \frac{\sigma_{3\alpha}}{\eta_R}, \tag{16}$$

where

$$\eta_R = \frac{E_m}{12(1-\nu_m)}\left[\frac{E_m(\alpha_m-\alpha_s)(T_H-T_L)}{(1-\nu_m)Y} - 2\right]^{-1}. \tag{17}$$

Eq. (16) has the same form as the linear ratcheting approximation deduced by Huang et al. [18] for metal film crawling, where a constant shear stress was applied at the interface. The constant η_R was named as ratcheting-viscosity in observation of the analogy between the ratcheting deformation and Newtonian viscous flow or linear creep.

A condition for the ratcheting deformation is implied by (17), namely

$$\frac{E_m(\alpha_m-\alpha_s)(T_H-T_L)}{(1-\nu_m)Y} > 2. \tag{18}$$

When condition (18) is not satisfied, for example, if the temperature range is too small, the metal deforms elastically after the first cycle and does not accumulate any plastic deformation. For the cases with $\alpha_s > \alpha_m$, the same result holds after replacing $\alpha_m - \alpha_s$ with $\alpha_s - \alpha_m$ in (17) and (18). Taking $E_m = 200$ GPa, $Y = 100$ MPa, $\nu_m = 0.25$, $\alpha_m - \alpha_s = 10^{-5}$ K^{-1}, and $T_H - T_L = 100$ K, we obtain $\eta_R = 33.3$ GPa per cycle.

Let v_α be the accumulated in-plane displacements of the metal. The plastic shear strain is, approximately, $\gamma_\alpha^p \approx \frac{\partial v_\alpha}{\partial x_3}$, where the in-plane variation of the displacements has been neglected. Substituting (11) into (16) and integrating with respect to x_3, we obtain that

$$\frac{\partial v_\alpha}{\partial N} = \frac{1}{\eta_R}\left(\tau_\alpha x_3 - \frac{\partial p}{\partial x_\alpha}\left(Hx_3 - \frac{1}{2}x_3^2\right)\right). \tag{19}$$

The boundary conditions for the displacements are: (1) the displacements are zero at the metal–substrate interface, i.e., $v_\alpha = 0$ at $x_3 = 0$; and (2) at the film–metal interface, by continuity, the in-plane displacements of the metal equal to the in-plane displacements of the film, i.e., $v_\alpha = u_\alpha$ at $x_3 = H$. Thus, the accumulation of the in-plane film displacements is

$$\frac{\partial u_\alpha}{\partial N} = \frac{1}{\eta_R}\left(\tau_\alpha H - \frac{H^2}{2}\frac{\partial p}{\partial x_\alpha}\right). \tag{20}$$

Furthermore, integration of (19) with respect to x_3 from 0 to H gives the in-plane plastic flow rates across the thickness. The mass conservation of plastic flow requires that

$$\frac{\partial H}{\partial N} = -\frac{\partial}{\partial x_\alpha}\left(\int_0^H \frac{\partial v_\alpha}{\partial N}\,dx_3\right). \tag{21}$$

Substituting (19) into (21) and noting that $H = H_0 + w$, we obtain that

$$\frac{\partial w}{\partial N} = \frac{1}{\eta_R}\frac{\partial}{\partial x_\alpha}\left[\frac{H^3}{3}\frac{\partial p}{\partial x_\alpha} - \frac{H^2}{2}\tau_\alpha\right]. \tag{22}$$

Eqs. (20) and (22), together with Eqs. (1) and (2), describe the displacement evolution of the elastic film as the temperature cycles. The equations are analogous to those obtained for an elastic film on a viscous layer [8], with the number of cycles N replacing the time t and the ratcheting viscosity η_R replacing the creep viscosity. Similar analogy has been used to understand metal film crawling and ratcheting-induced cracking [18,23,24]. In fact, Eq. (20) reduces to that for metal film crawling [18] when only a uniform shear traction acts at the metal surface. The present model suggests that a non-uniform shear traction causes the metal surface to undulate while crawling. Also interestingly, a uniform pressure at the surface does not cause any ratcheting deformation in the metal, but a non-uniform pressure induces both crawling and surface undulation. In all cases, a necessary condition for ratcheting deformation is given by Eq. (18).

As noted before, the model has several limitations. For example, the temperature-dependent material properties and strain hardening have been ignored. The thickness of the metal layer is assumed to be small compared to the wavelength of in-plane perturbation. Nevertheless, the mechanism is robust in that the metal layer ratchets as long as (i) the thermal expansion mismatch causes the metal to yield, and (ii) the plastic shear strain accumulates due to wrinkling perturbation. Consequently, the quatitative results should be used with caution, but the qualitative trends should be reliable.

3. Analytical solutions

The previous section develops a model for ratcheting-induced wrinkling, which is three-dimensional in general. To make the problem simpler, the remainder of this paper considers plane–strain deformation only. In this case, analytical solutions are available for linear perturbation analysis and constrained equilibrium states, analogous to those obtained in [8] for an elastic film on a viscous layer.

3.1. Linear perturbation analysis

Assume a sinusoidal wrinkle of small amplitude

$$w(x_1, N) = A(N)\sin\left(\frac{2\pi x_1}{\lambda}\right), \tag{23}$$

where $A(N)$ is the wrinkle amplitude, and λ the wrinkle wavelength. The perturbation in the in-plane displacement has a small effect on the result and will be ignored here. Refer to [8] for a full analysis.

Substituting (23) into (1), we obtain the pressure at the film–metal interface

$$p = \left[D_f\left(\frac{2\pi}{\lambda}\right)^4 + \sigma_0 h_f\left(\frac{2\pi}{\lambda}\right)^2\right]A\sin\left(\frac{2\pi x_1}{\lambda}\right), \tag{24}$$

where only the first-order terms of A is retained for linear analysis. The shear traction at the interface is zero because the in-plane displacement has been ignored.

Inserting (23) and (24) into (22), and again keeping only the first-order terms in A, we obtain the amplitude growth per cycle

$$\frac{dA}{dN} = s(\lambda)A, \tag{25}$$

where

$$s(\lambda) = \frac{H_0^3}{3\eta_R}\left(\frac{2\pi}{\lambda}\right)^4\left[-\sigma_0 h - D_f\left(\frac{2\pi}{\lambda}\right)^2\right]. \tag{26}$$

Note that, by neglecting the in-plane displacement, the growth rate (26) is four times faster than that in [8] at the limit of small underlayer thickness (i.e., $H_0 \ll \lambda$). Solving (25), we obtain that

$$A(N) = A_0\exp(sN), \tag{27}$$

where A_0 is the initial amplitude of the wrinkle.

Fig. 4 sketches the wrinkle growth rate s as a function of the wavelength for a compressively strained film ($\sigma_0 < 0$). The growth rate vanishes at a critical wavelength

$$\lambda_c = \frac{\pi h}{\sqrt{3(1-\nu_f^2)}}\sqrt{\frac{E_f}{-\sigma_0}}. \tag{28}$$

When $\lambda > \lambda_c$, $s(\lambda) > 0$ and the wrinkle amplitude grows exponentially. Otherwise, the amplitude decays. The critical wavelength is an outcome of the compromise between bending and in-plane deformation of the film. Upon wrinkling, the film relaxes the strain energy

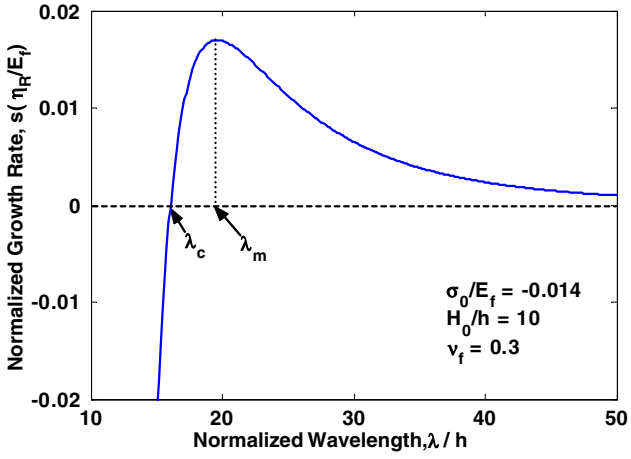

Fig. 4. Normalized growth rate as a function of the normalized wavelength.

associated with in-plane compression, but acquires some bending energy. The reduction of compression energy overcomes the bending energy for long wavelength, but the bending energy prohibits wrinkling of short wavelengths. The stability condition is identical to that of Euler buckling of a freestanding membrane [30] and to that of a compressed elastic film on a viscous layer [6–8]. The deformation of the underlayer, whether creeping or ratcheting, only affects the growth rate.

As shown in Fig. 4, for wrinkles with very long wavelengths, the growth rate diminishes. Growth of long-wavelength wrinkles requires plastic flow over a long distance in the metal layer and takes many cycles. As a result, the wrinkle grows the fastest at an intermediate wavelength

$$\lambda_{\mathrm{m}} = \frac{\pi h}{\sqrt{2(1-\nu_{\mathrm{f}}^2)}}\sqrt{\frac{E_{\mathrm{f}}}{-\sigma_0}}. \tag{29}$$

The corresponding growth rate is

$$s_{\mathrm{m}} = \frac{16\left(1-\nu_{\mathrm{f}}^2\right)^2(-\sigma_0)^3}{9\eta_{\mathrm{R}}E_{\mathrm{f}}^2}\left(\frac{H_0}{h}\right)^3. \tag{30}$$

We note that the wavelength of the fastest growing mode is independent of the metal layer. The growth rate in (30) increases as the thickness of the metal layer increases, which is only correct for a thin metal layer as assumed in this model. For a thick metal layer, the growth rate should approach an asymptote for infinite thickness, analogous to wrinkling on a thick viscous layer [6,37].

3.2. Constrained equilibrium states

For a compressed elastic film on a viscous layer, experiments have shown that wrinkles grow and attain an equilibrium amplitude after some time [33]. The analogy between creep and ratcheting suggests the same equilibrium state for ratcheting-induced wrinkles. The wrinkle reaches an equilibrium state when the tractions at the interface between the film and the metal layer vanish. At the equilibrium state, the metal undergoes cyclic plastic deformation with no ratcheting and the wrinkle does not grow. By setting $p = \tau_1 = 0$ in Eqs. (1) and (2), we obtain the equilibrium state:

$$w = A_{\mathrm{eq}}\sin\left(\frac{2\pi}{\lambda}x_1\right), \tag{31}$$

$$u_1 = -\frac{\pi}{4\lambda}A_{\mathrm{eq}}^2\sin\left(\frac{4\pi}{\lambda}x_1\right), \tag{32}$$

where

$$A_{\mathrm{eq}} = \frac{h}{\sqrt{3}}\sqrt{\left(\frac{\lambda}{\lambda_{\mathrm{c}}}\right)^2 - 1}. \tag{33}$$

Note that, at the equilibrium, the in-plane displacement undulates with half wavelength of the wrinkle, a result of non-linear behavior.

For any wavelength $\lambda > \lambda_{\mathrm{c}}$, Eq. (33) gives a real value for the equilibrium amplitude, and a non-trivial equilibrium state exists. Such an equilibrium state is similar to post-buckling of a column under an axial compression. For a blanket film, infinitely many such equilibrium states exist. The total strain energy in the film is lower for an equilibrium state with longer wavelength [8]. Consequently, the equilibrium state of a finite wavelength is energetically unstable. On the other hand, the ratcheting of the metal layer controls the kinetics. Near an equilibrium state, the wrinkle grows very slowly, thus kinetically constrained.

Combining the results from the linear perturbation analysis and the equilibrium states, one can envision the wrinkling process. Starting from a random perturbation, the fastest growing mode ($\lambda = \lambda_{\mathrm{m}}$) dominates the initial growth. The amplitude grows exponentially at the initial stage of cycling and then saturates at the equilibrium state. For the fastest growing mode, the equilibrium amplitude is, $A_{\mathrm{eq}} = h/\sqrt{6}$. Thereafter, the wrinkle evolves toward longer wavelength and larger amplitude to further reduce the elastic energy in the film, but very slow due to the kinetic constraint of ratcheting deformation in the underlying metal.

4. Numerical simulations

In this section, we simulate the wrinkling process by integrating Eqs. (22) and (20) numerically with a finite difference method. Consider plane strain deformation only. Start with a displacement field, $w(x_1)$ and $u_1(x_1)$ at cycle N. Eqs. (1) and (2) determine the tractions at the film–metal interface. The displacement field is then updated for the next cycle according to Eqs. (22) and (20). Repeat the procedure to evolve the displacement field over many cycles. The forward-time-centered-space (FTCS) differencing scheme is used. To ensure numerical stability, each cycle is broken into many small intervals. The equations are normalized so that only a small number of dimensionless parameters need to be specified.

4.1. Sinusoidal wrinkles

We first consider sinusoidal wrinkles. The initial condition is specified as a sinusoidal deflection with a small amplitude and zero in-plane displacement. The periodic boundary condition is assumed for this simulation. Fig. 5 shows the evolving displacements. Both the coordinate and the displacements are normalized by the film thickness. The following parameters were used in the simulation: $\sigma_0/E_{\mathrm{f}} = -0.014$, $A_0/h = 0.01$,

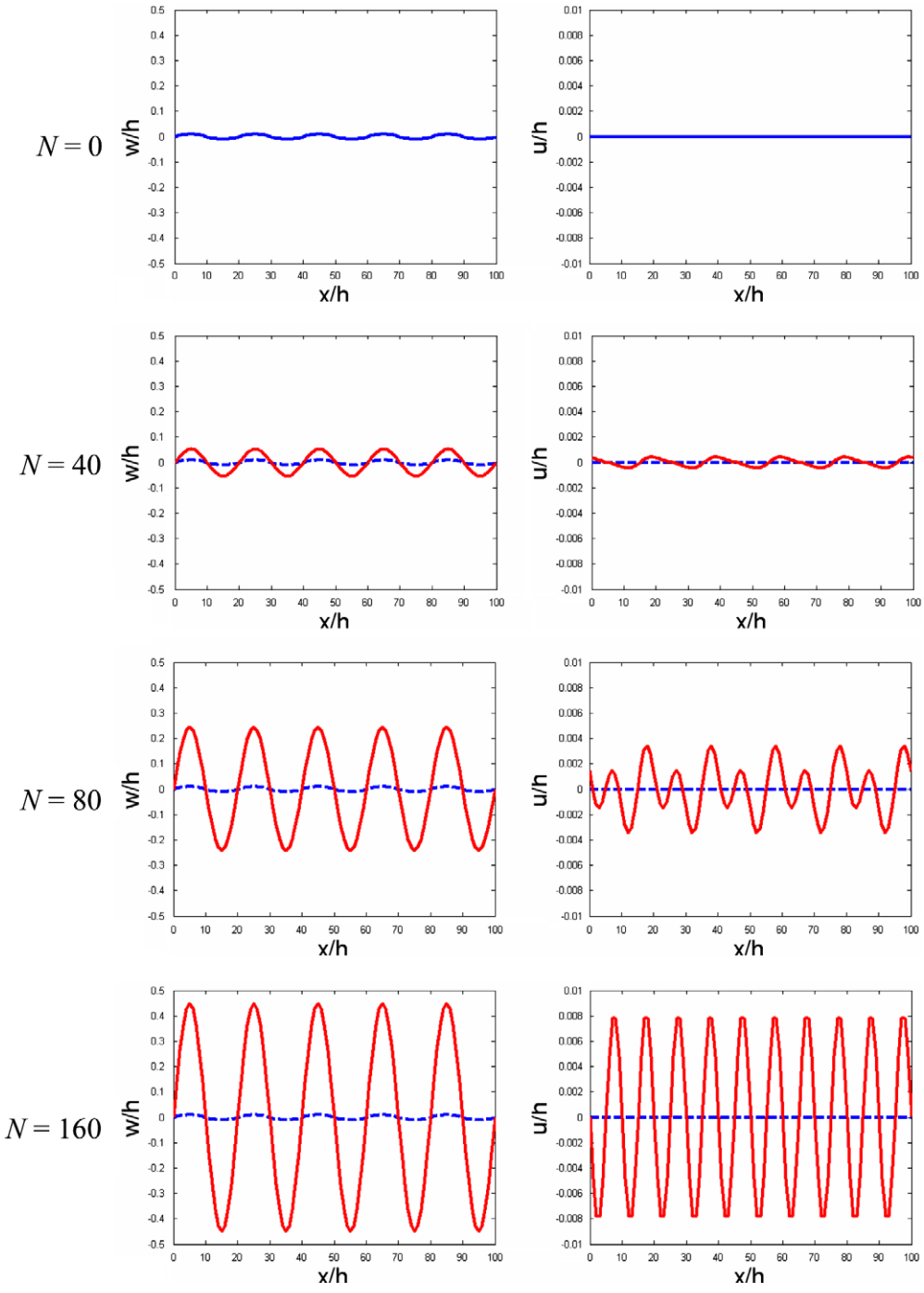

Fig. 5. Simulated evolution of the deflection and in-plane displacement of a sinusoidal wrinkle as temperature cycles.

$H_0/h = 10$, $\lambda/h = 20$, $\eta_R/E_f = 0.1$. The wavelength was selected to be close to the fastest growing mode to save computation time. As the temperature cycles, the wrinkle grows, accompanied by a small amount of in-plane displacement. Fig. 6 shows the wrinkle amplitude as a function of the number of cycles. Initially, the amplitude grows exponentially, following the prediction of linear perturbation analysis. After about 40 cycles, the wrinkle deviates from exponential growth and approaches the equilibrium state after about 120 cycles; the amplitude does not change significantly thereafter. Fig. 5 also shows that the in-plane displacement evolves from a wave of the wrinkle wavelength at the initial stage to a wave of half the wrinkle wavelength at equilibrium, as predicted by the analytical solution in Section 3. Although the equilibrium state is energetically unstable, subsequent evolution toward longer wavelengths is extremely slow due to the kinetic constraint of ratcheting,

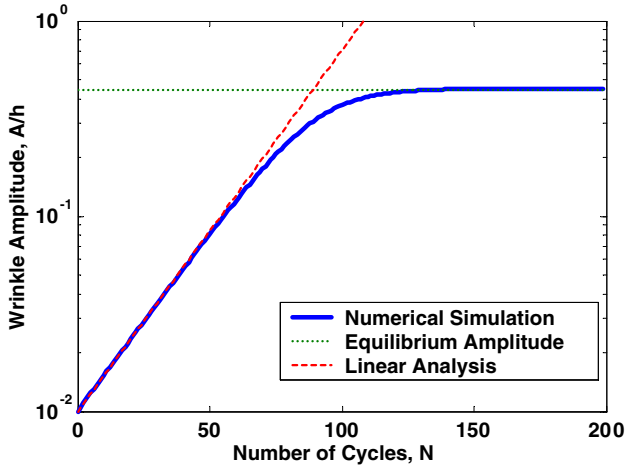

Fig. 6. Amplitude of a sinusoidal wrinkle as a function of the number of temperature cycles.

which was not observed in our simulations. A perturbation to the equilibrium state may be necessary to numerically trigger the evolution.

4.2. Wrinkling with elastic constraint

In a thermal barrier system (Fig. 1), the TGO film is under compression due to lateral growth at high temperatures. As temperature cycles, ratcheting of underlying bond coat allows the TGO film to grow wrinkles. The TBC layer on top, however, constrains upward deflection of the TGO film. Consequently, the wrinkle tends to grow into the bond coat. Fig. 7(a) shows a wrinkled TGO film in a thermal barrier system observed by Mumm et al. [26]. Fig. 7(b) sketches a model structure to be used for simulations. Assume a clamped boundary condition at both ends of the film. Within the span, the TBC layer provides an elastic constraint against upward deflection, but downward deflection is not constrained, resembling the case when the TBC layer is debonded from the TGO film due to interface cracking. Outside the span, the film is clamped between the bond coat and the TBC layer with perfect bonding. To approximate this elastic constraint, we add a term linearly proportional to the upward deflection to Eq. (1) for the pressure at the film–metal interface, namely

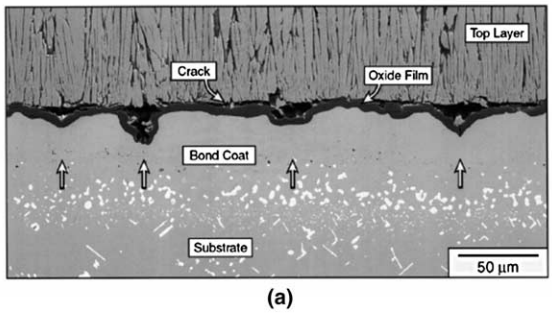

Fig. 7. (a) A thermal barrier system with wrinkled TGO film from [26]. (b) A model structure with elastic constraint on top of the film.

$$p = D_f \frac{\partial^4 w}{\partial x_\alpha \partial x_\alpha \partial x_\beta \partial x_\beta} - N_{\alpha\beta} \frac{\partial^2 w}{\partial x_\alpha \partial x_\beta} - \tau_\alpha \frac{\partial w}{\partial x_\alpha} - S w \hbar(w), \tag{34}$$

where $\hbar(w)$ is the heavyside function taking value 1 for positive w and 0 for negative w, and S is a parameter characterizing the stiffness of the elastic constraint. Rigorously, the additional pressure due to elastic deformation of the TBC layer is more complicated and depends on the elastic modulus and the thickness of the TBC layer. Our focus here is to illustrate the effect of an arbitrary elastic constraint on the wrinkling process by using the model structure and the above approximation. A more sophisticated analysis on the elastic constraint is in progress and will be reported elsewhere.

With Eq. (34) replacing Eq. (1), we simulate the wrinkling process with various degrees of elastic constraint. The initial condition is specified as a deflection described by a Gauss function, i.e.

$$w(x_1, N = 0) = -A_0 \exp\left(-\frac{x_1^2}{\Delta^2}\right), \tag{35}$$

where A_0 is the initial amplitude of the perturbation and Δ is the characteristic half width. In all simulations presented in this section, we start from the same initial perturbation with $A_0/h = 0.01$ and $\Delta/h = 20$. The length within the span of the model film is $200h$, the compressive stress in the film $\sigma_0/E_f = -0.014$, and the ratcheting viscosity $\eta_R/E_f = 0.1$.

Fig. 8 shows a simulation of the evolving displacement in the case of no constraint (i.e., $S = 0$). The dashed line in each plot shows the initial perturbation. Initially, the perturbation grows slowly, with the amplitude increasing and the width decreasing, consistent with mass conservation of the plastic deformation of the metal layer. After about 200 cycles, the wrinkle develops multiple waves, with the dominant wavelength close to the fastest growing mode predicted by linear perturbation analysis (see Eq. (29) or Fig. 4). Subsequent growth of the wrinkle is similar to that of a sinusoidal wrinkle as shown in Fig. 5, except that the film is now clamped at the both ends. Note that the wavelength after 5000 cy-

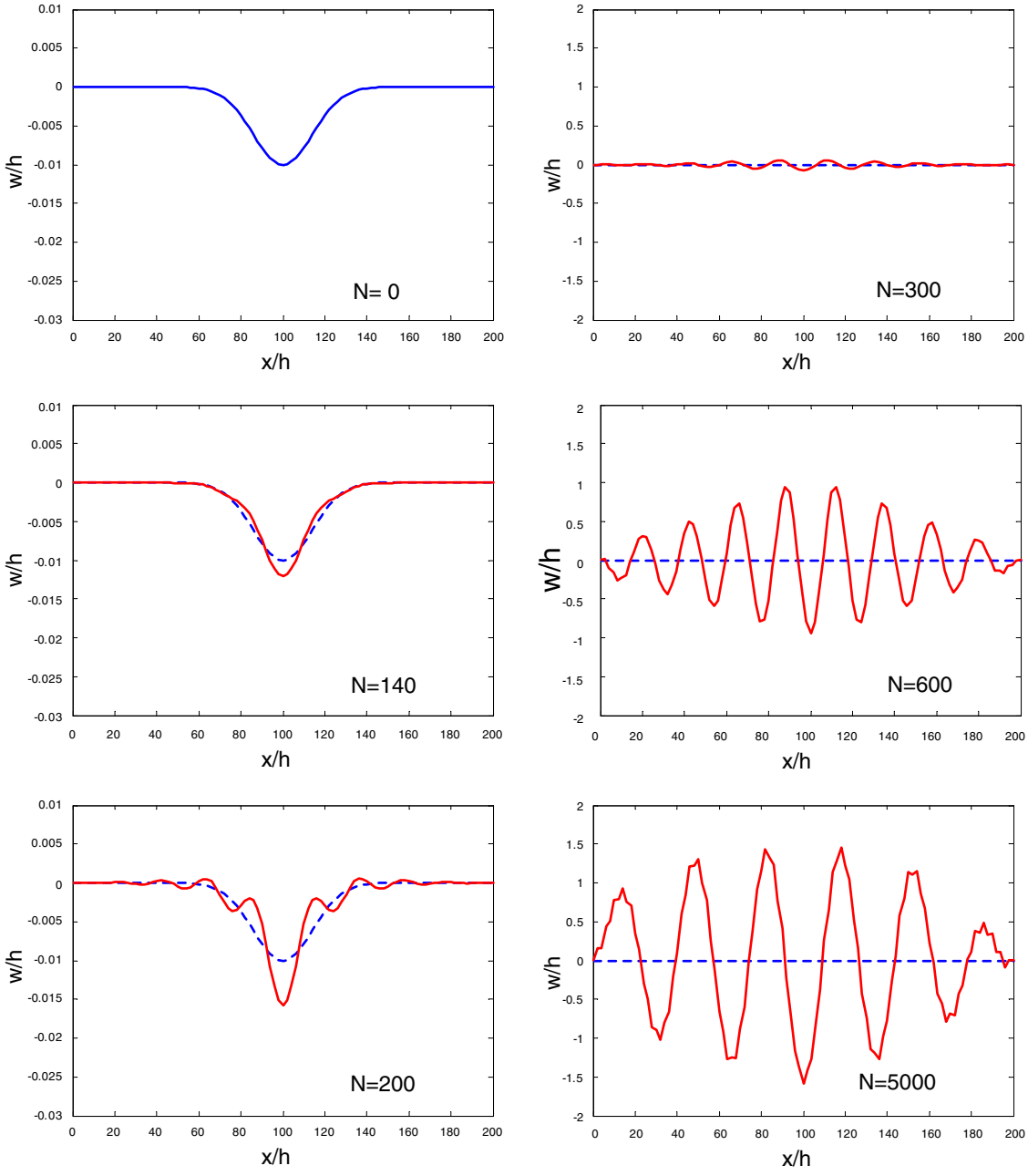

Fig. 8. Simulated evolution of wrinkling as temperatures cycles with no elastic constraint ($S = 0$).

cles is longer than that at 600 cycles, which is consistent with the fact that the elastic strain energy of the film decreases as the wavelength increases [8]. It is expected that both the wrinkle amplitude and the wavelength keep increasing as thermal cycling continues. Some numerical errors accumulate after integrating over a large number of cycles, as noted in Fig. 8 for $N = 5000$.

Fig. 9 shows the simulation with a small elastic constraint $S = 0.1E_f$. During the first 200 cycles, no significant upward deflection ($w > 0$) of the film occurs. Consequently, the evolution of the perturbation is similar to that in Fig. 8 for the elastic constraint is not a factor. After 200 cycles, however, as the film tends to wrinkle upward, the elastic constraint suppresses the development of multiple waves. The growth of wrinkles is constrained at the center portion of the film. After 5000 cycles, the perturbation evolves into a grooving shape, with small pile-up ridges at the top. Similar shapes have been obtained from finite element simulations [34].

Fig. 10 shows the simulation with a large elastic constraint $S = 10E_f$. Again, for the first 200 cycles, the behavior is similar to previous cases. After 200 cycles, the large elastic constraint almost completely suppresses the upward deflection. After 300 cycles, the wrinkle evolves into a shape with three peaks. It is interesting to

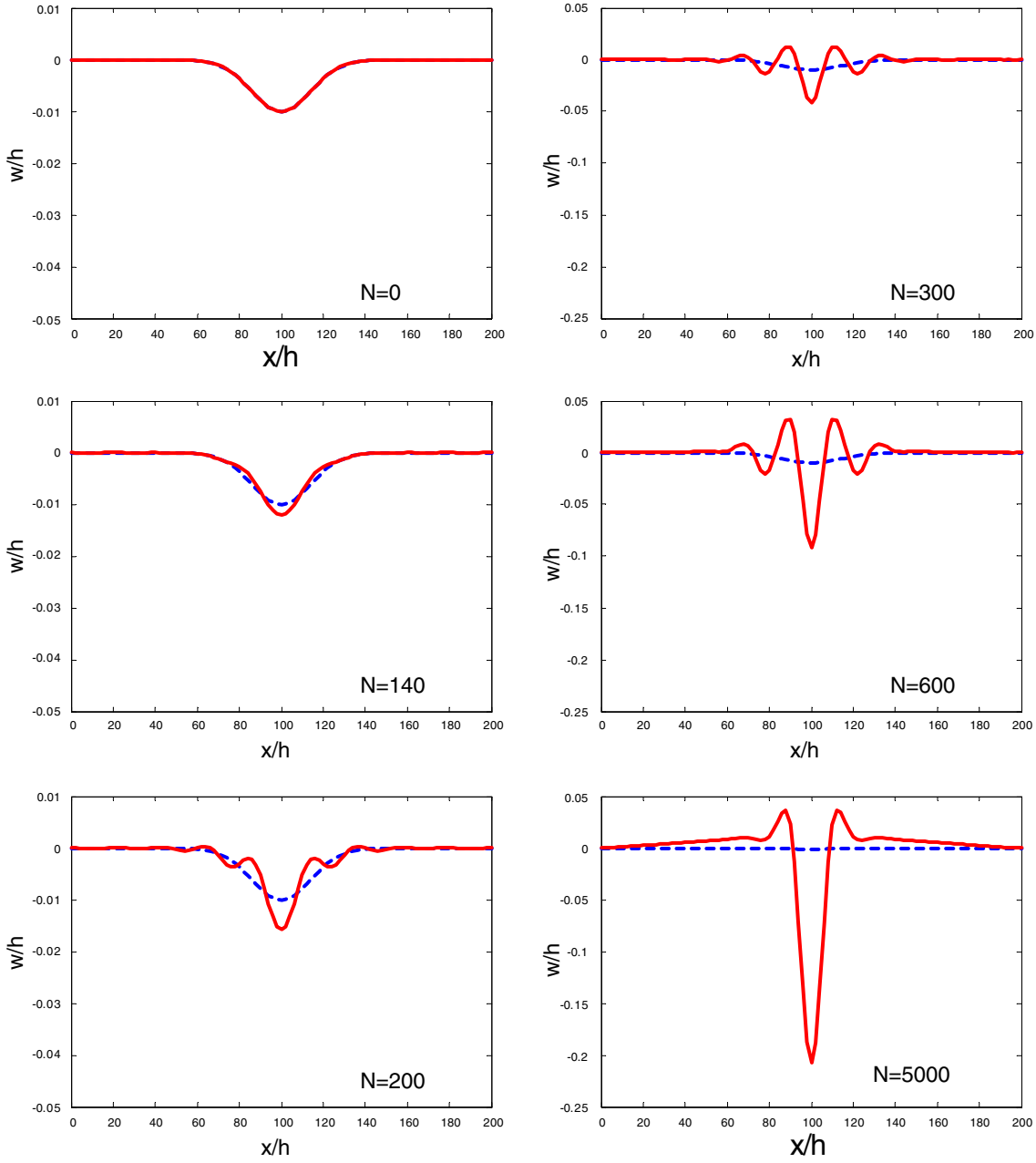

Fig. 9. Simulated evolution of wrinkling as temperatures cycles with elastic constraint $S = 0.1E_f$.

see that, after 600 cycles, the larger peak at the center grows deeper, with the smaller peaks consumed. In another simulation (not shown), we started from an initial perturbation with multiple peaks. As the temperature cycles, the growth of the peaks competed with each other; larger peaks grew and consumed smaller ones. Eventually, only one peak with a large amplitude remained. The implication of such behavior may be important for understanding the failure of thermal barrier systems: many small undulations of the TGO film may grow and merge into one big wrinkle to cause failure. The elastic constraint plays an important role in determining the profile of wrinkling.

Fig. 11 shows the wrinkle amplitude at the center as a function of temperature cycles for different stiffnesses of the elastic constraint. The results are essentially same for all simulations during the first 200 cycles, because of no significant upward deflection of the film and thus no effect of the elastic constraint. Without the elastic constraint ($S = 0$), after 200 cycles, the amplitude grows much faster than the initial stage, close to the fastest growth rate. After about 400 cycles, the growth slows down. However, due to the clamped boundary condition and the mass conservation of the metal layer, no analytical solution for equilibrium state exists, and the amplitude keeps increasing after many cycles, but very

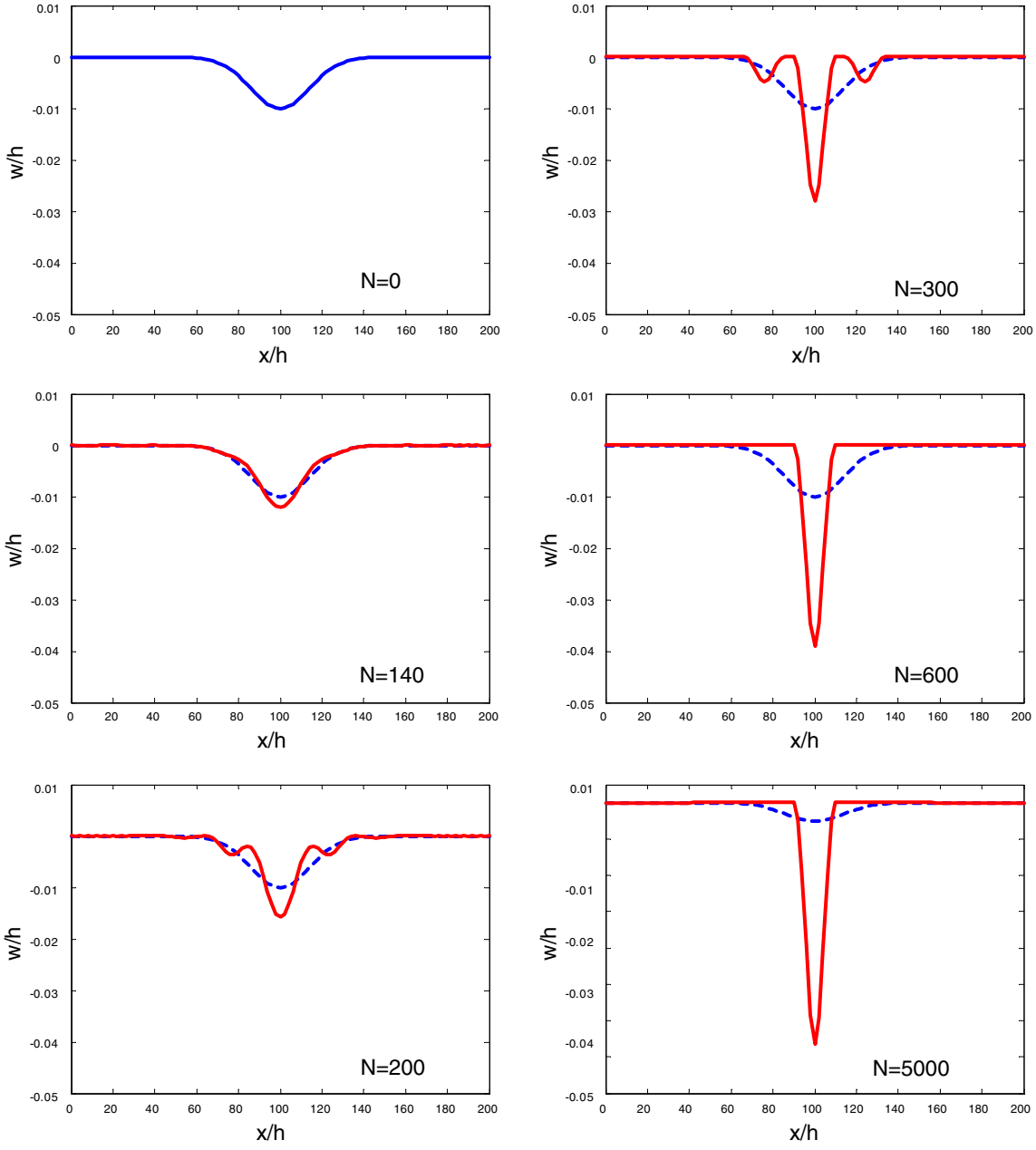

Fig. 10. Simulated evolution of wrinkling as temperatures cycles with elastic constraint $S = 10E_f$.

slowly, due to the kinetic constraint of ratcheting deformation underneath. With some elastic constraint, the amplitude growth is slower, but the amplitude after many cycles can be as large as that with no constraint. The stiffer the elastic constraint, the slower the wrinkle grows and the more cycles it takes to develop as large amplitude.

5. Discussions

The model developed in this study is to show the mechanism of ratcheting-induced wrinkling. Several approximations have been made during the course of model development. The temperature-dependent material properties and strain hardening have been ignored. The thickness of the metal layer is assumed to be small compared to the wrinkle wavelength. In thermal barrier systems, the oxide layer grows and deforms inelastically at high temperatures [26,27,34], and the metal bond coat creeps [10]. All these could affect wrinkling of the oxide film, making modeling the complete process a formidable task. Nevertheless, the present model provides interesting insight into a possible mechanism of wrinkling, not only for thermal barrier systems but also for other layered systems such as microelectronic interconnects with a passivation film on a metal conductor.

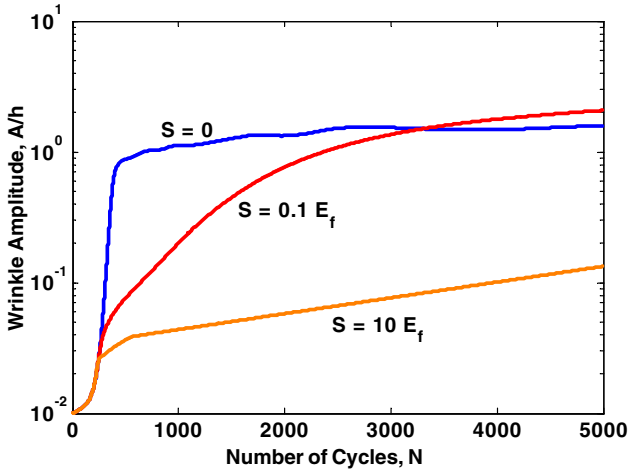

Fig. 11. The wrinkle amplitude as a function of the number of temperature cycles for various stiffness of the elastic constraint.

A previous study on thermal barrier systems showed that a critical undulation amplitude is required for ratcheting to occur [25]. In that case, the ratcheting was induced by the significant shear stress generated by the film undulation as temperature cycles, and the thermal mismatch between the metal layer and the underlying substrate was assumed negligible. The critical amplitude is relatively large, comparable to the wrinkle wavelength, which is unlikely at the initial stage. The present model assumes small amplitudes of wrinkling but large thermal expansion mismatches between the metal layer and the substrate. Under this condition, the metal ratchets without requiring any critical amplitude. Therefore, the present mechanism may be responsible for the initial growth of wrinkles.

One important consequence of wrinkling is the induced failure in layered structures. For example, the bending of the film may induce substantial tensile stress at the crest of wrinkles despite the fact that the average stress in the film is compressive [35,36]. A rough estimate can be made by considering the equilibrium state of a sinusoidal wrinkle. With the equilibrium amplitude given by Eq. (33), the maximum stress in the film is

$$\sigma_{\max} = \frac{E_f}{12(1-\nu_f^2)}\left(\frac{2\pi h}{\lambda}\right)^2\left[\sqrt{12\left(\frac{\lambda^2}{\lambda_c^2}-1\right)}-1\right]. \quad (36)$$

For the fastest growing mode ($\lambda = \lambda_m$), the stress is approximately $-1.3\sigma_0$, which is tensile and can be large enough to cause fracture. Wrinkle-induced fracture has been observed in a compressed elastic film on a viscous layer [36]. Another failure mode that can be induced by wrinkling is debonding at the interface. A previous numerical simulation showed that negative pressure of about 35 MPa could build up at the interface [35], which may be enough to cause debonding.

Numerical simulations in the present study have shown interesting features of wrinkling process, especially for the cases with elastic constraint from a top layer. The stiffness of the elastic constraint plays an important role in determining the wrinkling profile after many cycles. A sophisticated analysis is needed to better understand the effect of elastic constraint.

Acknowledgements

The work is supported by Advanced Technology Program of Texas Higher Education Coordinating Board. The authors thank Professor Z. Suo (Harvard University) and Professor A.G. Evans (University of California-Santa Barbara) for helpful discussions.

References

[1] Allen HG. Analysis and design of structural sandwich panels. New York: Pergamon Press; 1969.
[2] Bowden N, Brittain S, Evans AG, Hutchinson JW, Whitesides GM. Spontaneous formation of ordered structures in thin films of metals supported on an elastomeric polymer. Nature 1998;393:146–9.
[3] Huck WTS, Bowden N, Onck P, Pardoen T, Hutchinson JW, Whitesides GM. Ordering of spontaneously formed buckles on planar surfaces. Langmuir 2000;16:3497–501.
[4] Groenewold J. Wrinkling of plates coupled with soft elastic media. Physica A 2001;298:32–45.
[5] Hobart KD, Kub FJ, Fatemi M, Twigg ME, Thompson PE, Kuan TS, et al. Compliant substrates: a comparative study of the relaxation mechanisms of strained films bonded to high and low viscosity oxides. J Electron Mater 2000;29:897–900.
[6] Sridhar N, Srolovitz DJ, Suo Z. Kinetics of buckling of a compressed film on a viscous substrate. Appl Phys Lett 2001;78:2482–4.
[7] Sridhar N, Srolovitz DJ, Cox BN. Buckling and post-buckling kinetics of compressed thin films on viscous substrates. Acta Mater 2002;50:2547–57.
[8] Huang R, Suo Z. Wrinkling of an elastic film on a viscous layer. J Appl Phys 2002;91:1135–42.
[9] Serrano JR, Cahill DG. Micron-scale buckling of SiO_2 on Si. J Appl Phys 2002;92:7606–10.
[10] Balint DS, Hutchinson JW. Undulation instability of a compressed elastic film on a nonlinear creeping substrate. Acta Mater 2003;51:3965–83.
[11] Huang R. Kinetic wrinkling of an elastic film on a viscoelastic substrate. MSSM Report No. 04/01, The University of Texas at Austin.
[12] Suo Z. Wrinkling of the oxide scale on an aluminum-containing alloy at high temperatures. J Mech Phys Solids 1995;43:829–46.
[13] Isagawa M, Iwasaki Y, Sutoh T. Deformation of Al metallization in plastic encapsulated semiconductor devices caused by thermal shock. Proc Int Rel Phys Symp 1980:171–7.
[14] Thomas RE. Stress-induced deformation of aluminum metallization in plastic molded semiconductor devices. IEEE Trans Compon Hybr Manuf Technol 1985;8:427–34.
[15] Alpern P, Wicher V, Tilgner R. A simple test chip to assess chip and package design in the case of plastic assembling. IEEE Trans Compon Packag Manuf Technol A 1994;17:583–9. Corrections in 1995;18:862–3.

[16] Huang M, Suo Z, Ma Q, Fujimoto H. Thin film cracking and ratcheting caused by temperature cycling. J Mater Res 2000;15:1239–42.
[17] Huang M, Suo Z, Ma Q. Metal film crawling in interconnect structures caused by cyclic temperatures. Acta Mater 2001;49:3039–49.
[18] Huang M, Suo Z, Ma Q. Plastic ratcheting induced cracks in thin film structures. J Mech Phys Solids 2002;50:1079–98.
[19] Begley MR, Evans AG. Progressive cracking of a multilayer system upon thermal cycling. J Appl Mech 2001;68:513–20.
[20] Bree J. Elastic–plastic behavior of thin tubes subjected to internal pressure and intermittent high-heat fluxes with application to fast-nuclear-reactor fuel elements. J Strain Anal 1967;2:226–38.
[21] Jansson S, Leckie FA. Mechanical-behavior of a continuous fiber-reinforced aluminum matrix composite subjected to transverse and thermal loading. J Mech Phys Solids 1992;40:593–612.
[22] Suresh S. Fatigue of materials. 2nd ed. Cambridge: Cambridge University; 1998.
[23] Huang R, Prevost JH, Suo Z. Loss of constraint on fracture in thin film structures due to creep. Acta Mater 2002;50:4137–48.
[24] Liang J, Huang R, Prevost JH, Suo Z. Thin film cracking modulated by underlayer creep. Exp Mech 2003;43:269–79.
[25] He MY, Evans AG, Hutchinson JW. The ratcheting of compressed thermally grown thin films on ductile substrates. Acta Mater 2000;48:2593–601.
[26] Mumm DR, Evans AG, Spitsberg IT. Characterization of a cyclic displacement instability for a thermally grown oxide in a thermal barrier system. Acta Mater 2001;49:2329–40.
[27] Karlsson AM, Evans AG. A numerical model for the cyclic instability of thermally grown oxides in thermal barrier systems. Acta Mater 2001;49:1793–804.
[28] He MY, Hutchinson JW, Evans AG. Simulation of stresses and delamination in a plasma-sprayed thermal barrier system upon thermal cycling. Mater Sci Eng A 2003;345:172–8.
[29] Panat R, Zhang S, Hsia KJ. Bond coat surface rumpling in thermal barrier coatings. Acta Mater 2003;51:239–49.
[30] Timoshenko S, Woinowsky-Krieger S. Theory of plates and shells. 2nd ed. New York: McGraw-Hill; 1987.
[31] Landau LD, Lifshitz EM. Theory of elasticity. London: Pergamon Press; 1959.
[32] Hill R. The mathematical theory of plasticity. Oxford: Clarendon Press; 1950.
[33] Yin H, Huang R, Hobart KD, Suo Z, Kuan TS, Inoki CK, et al. Strain relaxation of SiGe islands on compliant oxide. J Appl Phys 2002;91:9716–22.
[34] Karlsson AM, Hutchinson JW, Evans AG. A fundamental model of cyclic instabilities in thermal barrier systems. J Mech Phys Solids 2002;50:1565–89.
[35] Liang J, Huang R, Yin H, Sturm JC, Hobart KD, Suo Z. Relaxation of compressed elastic islands on a viscous layer. Acta Mater 2002;50:2933–44.
[36] Yin H, Huang R, Hobart KD, Liang J, Suo Z, Shieh SR, et al. Buckling suppression of SiGe islands on compliant substrates. J Appl Phys 2003;94:6875–82.
[37] Huang R, Suo Z. Instability of a compressed elastic film on a viscous layer. Int J Solids Struct 2002;39:1791–802.